ACCSCIENCE PUBLISHING

International Journal of Bioprinting

RESEARCH ARTICLE

Biofabrication of tri-layered nerve guide conduits for peripheral nerve regeneration: Synergizing melt-electrowriting of polymeric fibers and extrusion-based 3D bioprinting

Jiarui Zhou[1,2], Kamil Elkhoury[1], Soja Saghar Soman[1], and Sanjairaj Vijayavenkataraman[1,2]*

[1]The Vijay Lab, Division of Engineering, New York University Abu Dhabi, Abu Dhabi, United Arab Emirates

[2]Department of Mechanical and Aerospace Engineering, Tandon School of Engineering, New York University, Brooklyn, New York, USA

Abstract

Nerve guide conduits (NGCs) are promising alternatives to autografts for the treatment of peripheral nerve injuries. These conduits are designed to replace the nerve tissue that has been damaged or removed from the injured nerve region. An ideal nerve conduit should effectively bridge the nerve gap and induce nerve cell growth and regeneration. Current FDA-approved NGCs predominantly address gaps smaller than 2 cm and are fabricated from rigid synthetic polymers. Nevertheless, cells prefer softer substrates that more closely mimic the extracellular matrix (ECM). While hydrogels emerge as an ideal ECM-mimicking material, their application is limited by challenges in suturing, maintaining structural integrity, and susceptibility to rapid biodegradation. In this study, we propose a tri-layered NGC biofabricated by combining melt-electrowriting (MEW) and extrusion-based bioprinting, thereby facilitating three functionalities—the outer layer of MEW-polycaprolactone (PCL) fiber monophasic structure for mechanical integrity, the middle layer of MEW-PCL aligned fibers providing topographical cues for axonal directionality, and the inner bioprinted gelatin methacryloyl layer for encapsulating cells in an ECM-mimicking matrix (~7 kPa stiffness matching nerve tissues). In addition to having tunable mechanical properties (by changing the outer layer design), these biocompatible materials are cost-effective, easily biofabricated, highly tunable for drug-loading, and can support the growth, proliferation, and differentiation of human neural stem cells to peripheral neurons, making the proposed tri-layered NGCs promising candidates for treating long nerve gap injuries.

Keywords: 3D bioprinting; GelMA hydrogel; Nerve guide conduit; Neural stem cells; Polycaprolactone fiber; Tissue engineering

***Corresponding author:**
Sanjairaj Vijayavenkataraman (vs89@nyu.edu)

Citation: Zhou J, Elkhoury K, Soman SS, Vijayavenkataraman S. Biofabrication of tri-layered nerve guide conduits for peripheral nerve regeneration: Synergizing melt-electrowriting of polymeric fibers and extrusion-based 3D bioprinting. *Int J Bioprint*. 2025;11(2):530-544. doi: 10.36922/IJB025040032

Received: January 23, 2025
Revised: February 12, 2025
Accepted: February 24, 2025
Published online: March 28, 2025

1. Introduction

The human peripheral nervous system plays a crucial role in controlling sensations, movement, and motor coordination throughout the body. Peripheral nerves can suffer damage from injuries or neurodegenerative diseases, and severe peripheral nerve injuries can result in the loss of neurological function, numbness, and muscle atrophy.[1] While various therapeutic approaches, including anti-inflammatory medications, physiotherapy, surgery, nerve grafting, and rehabilitation, have been proposed, only a few treatments effectively restore neurological function.[2–4] In many cases, damaged nerves need to be replaced with grafts.[5] Autografting, using a patient's own nerves as grafts, is considered the gold standard for treating damaged nerve gaps.[6] However, this approach involves injuring source nerves, which can cause donor site morbidity. Therefore, biofabricated peripheral nerve guide conduits (NGCs) offer a promising alternative as ideal nerve grafts to bridge severed nerve segments. Designing and bioprinting NGCs require comprehensive knowledge of neural architecture, injury type, neural support cells, suitable scaffold materials, and neural growth factors to optimize the mechanical properties of the conduit.[7] Developing NGCs that are physiologically and anatomically compatible is a challenging yet essential task for translational medicine applications.

In recent years, there has been a growing interest in naturally available compounds that can be modified to create crosslinkable and stable hydrogels.[8–10] These materials are appealing due to their ability to have tunable mechanical properties and high biocompatibility.[11] One of the most widely recognized natural compounds in this regard is gelatin, which is derived from collagen found in animal tissues. Gelatin can be modified into gelatin methacryloyl (GelMA) by adding methacryloyl groups to its molecules.[12] This modification enables GelMA to crosslink and form a stable hydrogel when exposed to ultraviolet (UV) light or other suitable crosslinking agents. Recent studies have demonstrated that GelMA hydrogel can support cell growth.[13,14] This is attributed to GelMA's ability to mimic the extracellular matrix (ECM) and its adjustable pore size, which promotes cell adhesion and proliferation. The versatility of GelMA, coupled with its biodegradability, capacity for drug encapsulation, and ease of 3D printing, positions it as a highly promising material for a wide spectrum of biomedical applications.[15] These applications encompass wound healing, cartilage repair, nerve regeneration, and drug delivery, highlighting GelMA's potential in advancing various areas of healthcare and medicine.[16]

The field of tissue engineering is experiencing significant advancements, with 3D printing technology playing a pivotal role in its expansion.[17] This technology is being employed for various purposes, including the creation of high-performance mechanical structures, the generation of micron-scale models, and the development of human organ models.[18] Among the techniques available for tissue engineering, melt-electrowriting (MEW) has gained widespread popularity due to its ability to produce robust and highly porous films.[19] MEW achieves this by utilizing micron-scale diameter fibers and creating intersections between multiple fibers. Through adjustment of printing parameters, MEW can achieve precise alignment and control over the fibers, resulting in thicknesses as fine as 5 μm.[20] MEW offers several advantages over other methods, such as melt electrospinning or commercially available extrusion-based 3D printing. These advantages include exceptional resolution and precision with intricate details, highly aligned fibers that can mimic the natural structures found in tissues like muscles, nerves, or blood vessels,[21] and the creation of highly porous structures suitable for applications like filtration and drug delivery.[22]

Synthetic polymer-based NGCs made of purely synthetic polymers such as polycaprolactone (PCL), polylactic acid (PLA), and poly(lactide-co-ε-caprolactone) (PLCL) have been substantially investigated in previous published works, but they do not provide an ECM-mimicking microenvironment to either encapsulate the cells or for the cells *in vivo* to thrive and their stiffness is significantly higher than that of the native tissues.[23] On the other hand, NGCs made of pure natural polymers such as collagen or gelatin, despite providing an ECM-mimicking microenvironment, suffer rapid degradation and have inadequate mechanical stability when it comes to making longer conduits for treating long nerve gap injuries.[24] Therefore, it is crucial to create hybrid multi-layered NGCs from both soft and hard biocompatible materials. The goal is to simulate the ECM environment while ensuring sustained structural integrity for the duration of the nerve regeneration process.

Previously, multi-layered NGCs, including combinations such as hydrogel–hydrogel, polymer–hydrogel, and polymer–nanospheres, have been developed to offer superior structural support and optimal conditions within the channels for promoting neurite outgrowth *in vivo*.[25–27] For example, Takeya et al.[25] reported a two-layer NGC with an outer layer of chitosan and an inner layer of collagen. However, the aim of using the outer chitosan layer was to promote axonal regeneration and not to improve the mechanical properties of the conduits. The conduit was only 2 mm in length; the same material combination might fail when it comes to centimeter-scale conduits as both chitosan and collagen are soft polymers. Another approach is to have an outer synthetic polymer layer and

an inner hydrogel layer. For example, Lee et al.[26] fabricated a two-layer NGC with an outer electrospun PLCL layer and an inner gelatin layer. However, the outer electrospun layer had a random fibrous structure with unpredictable mechanical properties that would hinder the directional alignment of axons during neural regeneration.

In this study, we report a biofabricated tissue-engineered tri-layered NGC. The outer layer is made of melt-electrowritten PCL with a primary design aim of mechanical stability. To this end, following three distinct design patterns were explored: square, horizontal diamond, and vertical diamond. The middle layer also consists of melt-electrowritten PCL but was unidirectionally aligned, with the primary aim being the directional alignment of axons. The inner layer was the ECM-mimicking neural stem cells (NSCs)-laden GelMA fabricated using extrusion-based bioprinting. These biofabricated tri-layered conduits were comprehensively characterized for their mechanical properties, subjected to *in vitro* culturing, and assessed for NSCs viability, proliferation, and differentiation into peripheral neurons.

2. Materials and methods

2.1. Materials

Polycaprolactone pellets with an average Mn 45,000, gelatin from porcine skin (type A, 300 bloom), methacrylic anhydride (MA), collagenase type II (C2-22-1G), and DAPI (D9542-5MG) were purchased from Sigma Aldrich (Burlington, USA). Lithium phenyl (2,4,6-trimethylbenzoyl) phosphinate (LAP) was purchased from Advanced BioMatrix (San Diego, USA). iPSC-derived Normal Human NSCs and NSC Growth Medium (500 mL) were purchased from AddexBio (San Diego, USA). AlamarBlue™ HS Cell Viability Reagent and LIVE/DEAD™ Viability/Cytotoxicity Kit (for mammalian cells) were purchased from Invitrogen (Waltham, USA). Paraformaldehyde 1% and glutaraldehyde 2% in 0.1 M phosphate buffer were purchased from UTECH (Schenectady, USA). B-27™ Supplement (50×, serum-free, 10 mL, 17504044) and GlutaMAX™ Supplement (100 mL, 35050061) were purchased from Gibco (New York, USA). Tween-20 (BP, Ph. Eur., USP/NF grade, GE1584) was purchased from Glentham Life Sciences (Corsham, UK). Anti-neurofilament heavy polypeptide antibody (50 µL, ab8135) and goat anti-rabbit IgG H&L (Alexa Fluor® 488, 500 µg, ab150077) were purchased from ABCAM (Cambridge, UK). Neurobasal™ Medium (500 mL, 21103049), SSIV VILO Mastermix with Ezdnase (11766050), and Powerup SYBR Master Mix (A25776) were purchased from Thermo Fisher Scientific Inc. (Waltham, USA). RNeasy Mini Kit (74104) was purchased from QIAGEN N.V. (Venlo, the Netherlands). Primers for *PRPH*, *TUBB3*, *NEFH*, *HNK1*, and *GAPDH* were purchased from BGI Genomics (Shenzhen, China).

2.2. Design and mechanical characterization of the PCL structural support layer

RegenHu discovery bioprinter (Switzerland) was used for MEW printing. Polycaprolactone pellets with an average Mn of 45,000 were directly loaded into the cartridge. G24L15M metal needles with an inner diameter of 0.28 mm were used. After the optimization process, 85 °C, 4 mm needle-to-substrate distance, 0.125 MPa pressure, 4.5 kV applied voltage, and 20 mm/s feed rate were applied in MEW producing straight and controllable aligned fibers.

Both ANSYS simulations and practical tensile tests were performed to evaluate the mechanical properties of different monophasic designs. The simulations were performed using ANSYS 2020 (Ansys, Inc., Canonsburg, USA), where 3D structures of identical dimensions were designed. A mesh size of 0.05 mm was employed, ensuring element quality >0.95. One end of the structure was set to be "fixed support," while the reaction force at the other end was calculated and exported. Stress–strain curves and Young's modulus were calculated and subsequently compared. Instron Universal Testing System – 5965 (Canton, USA) with 100 N load cell was used to perform the tensile test. The tensile specimen dimensions are 40 mm × 10 mm, with a gauge length of 20 mm. The test was conducted at a strain rate of 5 mm/min, and it was continued until the structure was fractured into two parts, at which point the force reached zero.

2.3. GelMA synthesis and hydrogel fabrication

GelMA was synthesized in accordance with the established procedures.[28] Briefly, gelatin from porcine skin was dissolved in Dulbecco's phosphate-buffered saline (DPBS) to reach a final concentration of 10% w/v while stirring at 50 °C for 1 h. To each gram of gelatin, 800 µL of methacrylic anhydride (Sigma-Aldrich) was added dropwise. The chemical reaction was allowed to take place while stirring at 50 °C for 2 h (Figure 1). The termination of the reaction was achieved by adding twice the initial volume of DPBS. To eliminate any excess methacrylic anhydride, the methacrylated gelatin solution was subjected to dialysis for 5 days with frequent water changes and then lyophilized. To prepare the hydrogels, 5% w/v GelMA was mixed with 0.25% w/v LAP and subsequently crosslinked using UV light (Form Cure, LED power 39 W, Formlabs Inc., Somerville, USA) for 90 s at 405 nm.

2.4. Rheology characterization of GelMA solution

Dynamic mechanical analysis (MCR 702e MultiDrive, Anton Paar Inc., Graz, Austria) was used to perform the rheology test of 5% w/v GelMA solution (before

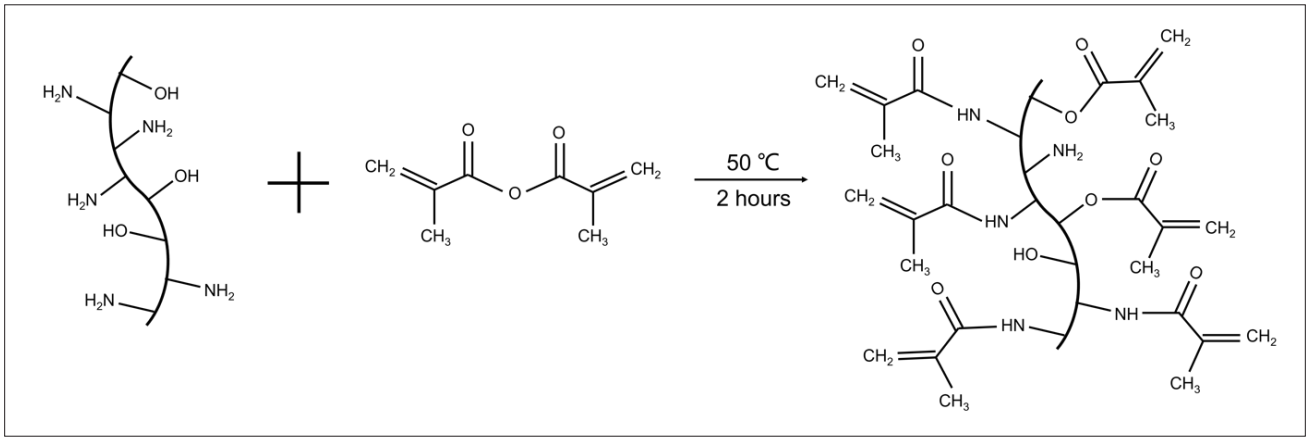

Figure 1. The chemical reaction between gelatin and methacrylate anhydride for the fabrication of gelatin methacryloyl (GelMA).

crosslinking). The linear viscoelasticity range was established through an amplitude sweep spanning from 0.1% to 1000%. Subsequently, the maximum linear viscosity value was identified, and a frequency sweep ranging from 0.1 to 100 Hz was conducted, employing a strain level below the maximum linear viscosity, to determine the shear storage modulus, shear loss modulus, and complex viscosity.

2.5. Scanning electron microscopy analysis

The MEW-printed PCL fibers and the porous structure of GelMA hydrogels were investigated with scanning electron microscope (SEM). PCL fibers were printed on top of a transparent glass slide and then directly imaged with FEI Quanta 3D FEG Dual Beam Electron Microscope (FEI Company, Hillsboro, USA) at 5 kV. The mean thickness of the MEW-printed PCL fibers was obtained from a group of three samples for each pattern (n = 50). A frequency distribution was generated, followed by plotting a histogram of the frequency distribution. A non-linear fit using a Gaussian distribution was then applied to the histogram. The GelMA hydrogel samples were lyophilized and subsequently cut to obtain the cross-section area. The cross-section areas were imaged at 5 kV. The mean sizes of the GelMA hydrogel pores were analyzed from a group of three samples (n = 50). The SEM images of the assembled tri-layer structures with and without the GelMA hydrogel were obtained at 10 kV. Sputter gold coating was performed before image capture to increase the electron density of all samples.

2.6. Mechanical characterization of GelMA hydrogel

Mach-1 v500cs (Biomomentum Inc., Laval, Canada) was used to perform the compression test and repeatability test (fatigue test). A 5% w/v GelMA hydrogel cylinder with a flat surface finish was fabricated and UV-crosslinked. We used an *in situ* crosslinking method with a pre-designed mold featuring flat top and bottom surfaces to ensure homogeneous contact between the hydrogel and the compression plate. The hydrogel thickness was controlled by the mold height for consistency. The hydrogel thickness was assessed using the Mach-1 machine. An optimized total strain of 15% thickness and a strain rate of 10% thickness per second were applied to all samples. To assess repeatability, the same compression test was conducted for 1500 cycles while maintaining a high-humidity environment to prevent the hydrogel from drying out.

2.7. Bioink preparation

5% w/v GelMA and 0.25% w/v LAP were directly mixed with NSC cell culture media at 37 °C in the dark. An extra 100 µL NSC suspension with a density of 2.0×10^6 cells/mL was added and gently mixed with the GelMA hydrogel. Subsequently, the GelMA bioink was extruded onto the PCL fibers and subjected to UV crosslinking for 90 s at a wavelength of 405 nm. A total of 1 mL bioink was prepared, which was enough to print 10 samples, resulting in 100 µL GelMA bioink and 2.0×10^5 cells per sample.

2.8. Biofabrication of tri-layered NGC

Overall, the design of scaffolds can be divided into following three layers: structural support fibers, aligned fibers, and a uniform hydrogel coating. First, three exemplary monophasic scaffolds, including square, horizontal diamond, and vertical diamond patterns, were printed with MEW as the structural support layer. Subsequently, horizontal struts with a line spacing of 0.5 mm were printed as the middle layer using MEW. GelMA bioink was extruded on top of the PCL fibers and then crosslinked to form a uniform hydrogel coating. Finally, the structures were folded manually into cylinders and sealed

with a fibrin glue sealant (Tisseel, Baxter International Inc., Deerfield, USA).

2.9. *In vitro* cell culture of tri-layered NGC

The tri-layered NGCs were cut into 8 mm length and 5 mm diameter and placed in 24-well plates. The tri-layered NGCs were washed one time with prewarmed phosphate-buffered saline (PBS) and one time with the NSC medium. NSC media (500 µL) was added to each well and the plates were incubated at 37 °C in a 5% CO_2 incubator. Media changes were performed once every 3 days for 2 weeks. The samples were analyzed for cell viability and cell proliferation on days 1, 7, and 14.

2.10. Cell viability in cultured tri-layered NGCs

Cell viability within the cultured tri-layered NGCs was assessed on days 1, 7, and 14 using the Live/Dead cell viability assay. The staining mix was prepared by combining 1 µL of calcein AM and 4 µL of ethidium homodimer-1 with 2 mL of PBS. The NGCs were rinsed with prewarmed PBS prior to staining. Following this, the staining solution was applied to the scaffolds in the well plate and incubated for 30 min at 37 °C. Post-incubation, the tri-layered NGCs were removed from the well plate, carefully opened, laid out on a glass slide, and imaged using a ZOE Fluorescent Cell Imager (Bio-Rad Laboratories Inc, Hercules, USA). The analysis and quantification of live and dead cells were performed using ImageJ software (National Institutes of Health, MD, USA).

2.11. Cell proliferation in cultured tri-layered NGCs

Cell viability and proliferation were quantified using the AlamarBlue assay (Days 1, 7, and 14). The process began by discarding the culture medium from the tri-layered NGCs, followed by the addition of prewarmed fresh medium mixed with AlamarBlue reagent at a 10:1 ratio into each well. The NGCs were then incubated in the dark for 4 h. From this mixture, 100 µL samples were collected thrice and stored at −80 °C until all designated time points were sampled. The absorbance readings of these samples were later acquired using a microplate reader (BioTek Instruments, Inc., Winooski, USA) at 570 nm, using 600 nm as the reference wavelength. The AlamarBlue reduction percentage, serving as an indicator of cell culture proliferation, was determined by applying the colorimetric equations provided by BioRad.

2.12. Cell differentiation in cultured tri-layered NGCs

After 7 days of culture, the NSC medium was replaced with the peripheral nerve (PN) induction medium. The PN induction medium was made by supplementing neurobasal media with 2 mM GlutaMAX™ and 2% B27 for differentiation of NSCs to PN.[29] Both the NSC medium and the PN induction medium were changed every 3 days. The tri-layered NGCs were cultured in the PN induction medium for another 14 days with PN differentiation analysis on Days 3 and 14 after induction.

2.13. Immunocytochemistry of PN protein marker

Immunocytochemistry of the PN protein marker was examined on Day 14 after induction. The tri-layered NGCs were stabilized with 4% paraformaldehyde for 10 min at room temperature. Following fixation, the cells underwent permeabilization with 0.1% Triton X-100 in PBS for 15 min, followed by three washes in 0.05% Tween-20 in PBS, and were then treated with 1% bovine serum albumin (BSA) for 1 h to prevent non-specific attachment. Afterward, the scaffolds were exposed to rabbit anti-neurofilament heavy polypeptide (NEFH) antibody (diluted 1:100 in 1% BSA in PBS) at room temperature for 1 h. The scaffolds were then rinsed three times in PBS and treated with the fluorescently tagged secondary antibody, Alexa Fluor® 488 Goat Anti-Rabbit IgG H&L (diluted 1:200 in 1% BSA in PBS) for 1 h at ambient temperature, followed by counterstaining with DAPI at a concentration of 1 µg/mL. Images were captured using a Leica SP8 confocal laser scanning microscope (Leica Microsystems, Wetzlar, Germany) for subsequent analysis.

2.14. mRNA expression of PN markers

The tri-layered NGCs were incubated in 1 mg/mL collagenase type II for 1 h at 37 °C to degrade the hydrogel and release the cells. RNA extraction was performed utilizing an RNeasy Mini Kit, followed by quantification using a Nanodrop ND-1000 spectrophotometer (Nanodrop Technologies LLC, Wilmington, USA). Subsequently, 120 ng of RNA underwent reverse transcription to cDNA via SSIV VILO Mastermix with Ezdnase. For real-time quantitative polymerase chain reaction (PCR), reactions were executed in triplicate using 8 ng of cDNA per reaction with Powerup SYBR Master Mix on a StepOnePlus Real-Time PCR System (Applied Biosystems, Waltham, USA). The mRNA levels of neural markers were assessed after differentiation induction on days 3 and 14, focusing on (i) the pan-neuronal marker tubulin beta 3 class III (*TUBB3*), (ii) two peripheral neuron (PN)-specific markers: peripherin (PRPH) and neurofilament heavy polypeptide (*NEFH*), and (iii) the stemness marker human natural killer 1 (HNK1). The sequences of the forward and reverse primers of genes analyzed were derived from our previous work.[30] The target gene expression was normalized to the expression level of the housekeeping gene *GAPDH* (glyceraldehyde 3-phosphate dehydrogenase). The results were expressed as relative mRNA expression compared to the Day 3 samples.

2.15. Statistical analysis

All experiments were conducted in triplicates using independent samples per condition, except for pore size

measurements where $n = 50$ was considered, ensuring reproducibility and statistical significance. All data are expressed as mean ± standard deviation. Statistical analyses were implemented by utilizing the one-way or two-way analysis of variance (ANOVA) to evaluate significance levels. Significance was indicated as ns (not significant), * ($p < 0.05$), **($p < 0.01$), and *** ($p < 0.001$).

3. Results and discussion

In this study, we developed a tri-layered NGC by combining MEW and extrusion-based bioprinting, thereby facilitating three functionalities—the outer layer of MEW-PCL fiber monophasic structure for mechanical integrity, the middle layer of MEW-PCL aligned fibers for axonal directionality, and the inner bioprinted GelMA layer for encapsulating cells in an ECM-mimicking matrix. The use of 3D printing for NGCs offers customizable features, operational ease, and precise control over structural configurations. While various fabrication techniques for NGCs have been explored, including polymer melt electrospinning and hydrogel-based 3D printing,[31,32] few have achieved the micro-scale complex patterns and ECM-mimicking cell-friendly substrate provided by the combination of MEW and extrusion-based bioprinting.

3.1. Optimal design of the outer structural support layer

We utilized the MEW system to fabricate three monophasic PCL-based patterns, including square, horizontal diamond, and vertical diamond. We first designed and printed these patterns (part i in Figure 2a–c), intended to serve as the outer layer of the tri-layer scaffold, thereby ensuring its structural integrity. The precision and uniformity of the

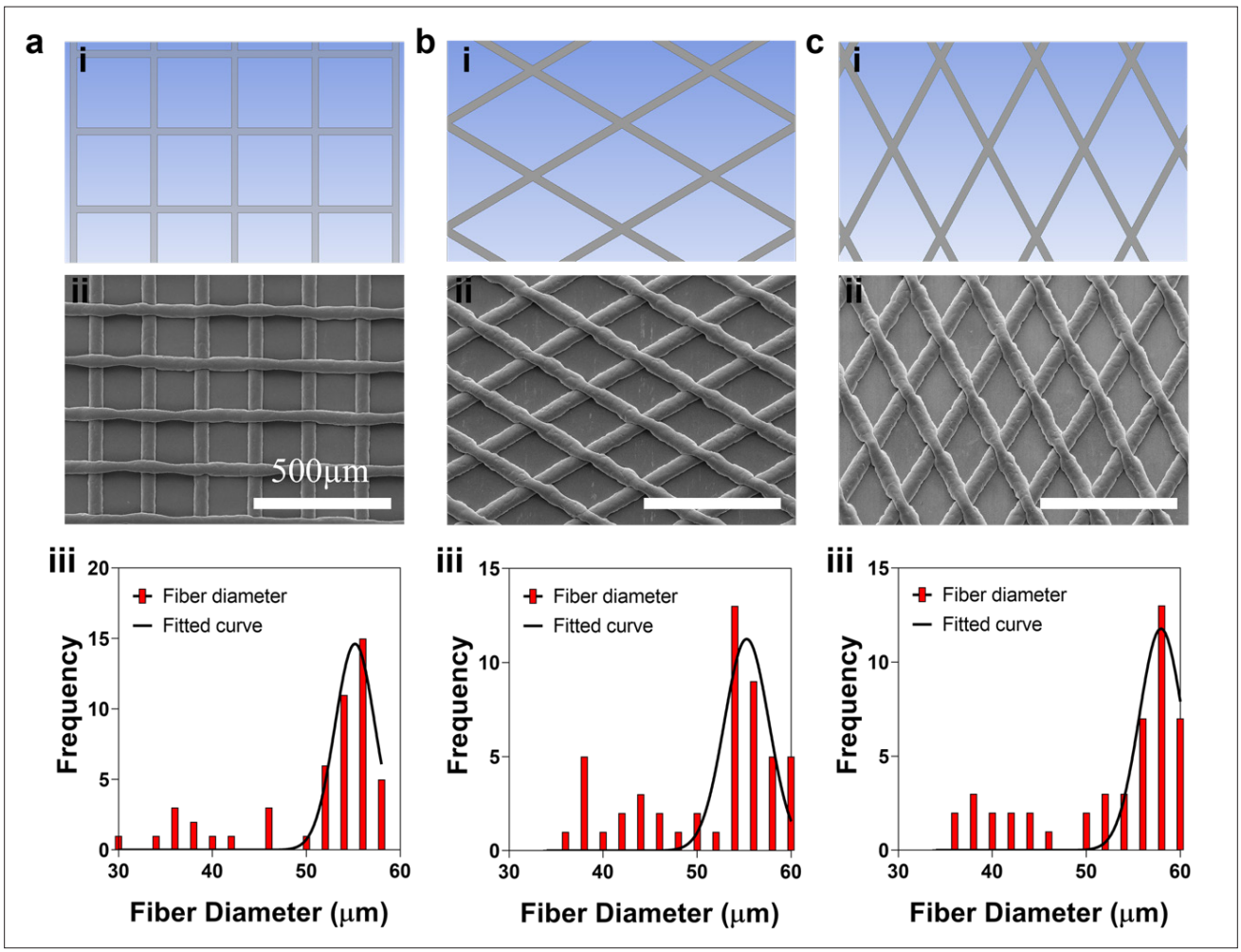

Figure 2. The CAD design (part i), SEM images of MEW-printed scaffolds (part ii), and fiber diameter distribution of MEW-printed PCL fiber (part iii) of the square (a), the horizontal diamond (b), and the vertical diamond patterns (c). Abbreviations: CAD, computer-aided design; MEW, melt-electrowriting; PCL, polycaprolactone; SEM, scanning electron microscopy.

fiber deposition process were evaluated by means of SEM images (part ii in Figure 2a–c). The examination of the fiber diameters, as shown in part iii in Figure 2a–c, reveals that despite the varied geometric configurations, the diameter distribution of MEW-printed PCL fibers across all three patterns remains consistently within the range of 50–60 μm. This observation underscores the excellent stability and reproducibility of MEW-printed PCL fibers across different pattern designs.

Figure 3a–c (parts i–iii) shows the geometry, equivalent stress, and equivalent strain of three distinct patterns obtained from the ANSYS simulation. Part iv in Figure 3a–c shows the exact region of the maximum stress, which is identical to the fracture area (experimental tensile test) in vi. Parts vi and v in Figure 3a–c show the images at the start and end of the experimental uniaxial tensile test. The maximum stress region obtained from the simulation result is the same fracture area observed from practical tensile experiments, proving the integrity of the mechanical performance of three distinct patterns (parts iv and v in Figure 3a–c). Figure 3d shows the stress–strain curves of the three distinct patterns obtained from the ANSYS simulation. The square pattern has the highest yield strength, while the horizontal diamond pattern achieves the lowest yield strength within a confined 5% strain.

Then, three monophasic patterns were printed and subsequently tested for their tensile properties at the same strain rate. Figure 3e illustrates the stress–strain curves of the three distinct patterns ($n = 3$). The horizontal diamond was found to be the most ductile pattern with a fracture point at around 95% elongation, while the vertical diamond achieved the highest ultimate tensile strength of around 2 MPa. As displacement increases at a constant rate, PCL fibers are elongated, and their pore size is enlarged. Fibers start to break and fracture after reaching the maximum force. In addition, the obtained linear elastic modulus of each design showed a high agreement with its Young's modulus result calculated from the ANSYS simulation (Figure 3f). This further solidifies the distinct mechanical performance of the three scaffold patterns.

Considering that Young's modulus of peripheral nerve tissue typically falls within the range below 10 MPa, and considering the potential torsion, stretching, and bending that may occur *in vivo* post-implantation, the horizontal diamond pattern is better suited to meet these requirements and has been chosen as the structural support layer for the tri-layered NGC.[33,34] This also brings in the inherent advantage of tunability. Depending on the size, morphology, site of injury, or age of the patient, the properties of NGCs can be tuned, if required, offering patient-specific customization.

3.2. GelMA offers a mechanically robust ECM-mimicking environment

Recent advancements have seen significant interest in 3D-printed/bioprinted hydrogels for tissue engineering due to their biomimetic properties, tunable mechanics, and ease of fabrication.[35] Specific to nerve tissue engineering, GelMA hydrogel has gained attention for its biocompatibility and ability to support NSC differentiation and promote neurite outgrowth and myelination.[36] For instance, Ye et al.[37] reported the fabrication of a multi-channel NGC using light-based 3D printing with GelMA. They successfully printed a 4-channel NGC with high printing fidelity, demonstrating GelMA's potential for NGC fabrication.

In Figure 4a, the three-interval thixotropy test demonstrates the stability and rapid recovery of 5% GelMA solution at a high shear rate of 100 Hz and a low shear rate of 0.1 Hz. Furthermore, Figure 4b shows that as the strain rates are increasing, the viscosity is decreasing which shows that the GelMA solution displayed a shear-thinning behavior, as the viscosity is highly dependent on the shear rate. It can be concluded that 5% GelMA solution is an ideal material for extrusion-based 3D printing due to the shear-thinning property and it can maintain the structural integrity during the post-printing process owing to the rapid recovery from high shear rate to low shear rate.

GelMA is a widely used photo-crosslinkable biomaterial and its crosslinking reaction can be activated by the presence of photo-initiators and proper light irradiations.[38] Figure 4c illustrates the significant rise in storage modulus following UV crosslinking for 120 s. The 5% GelMA solution was allowed to stabilize for 2 min before the UV light was switched on, and the experiment was continued for another 6 min after the UV light was turned off.

The pore size of hydrogels is crucial for enhancing cell adhesion and proliferation.[39] Hydrogels with their intrinsic porous structures facilitate complicated interactions between the cell surface and the adhesive properties or ligands of substrates.[24] Insufficiently small pores hinder cell migration through the 3D scaffolds, while excessively large pores reduce the available specific surface area, thereby impairing cell attachment.[40] A proper pore size is important for cell adhesion and proliferation in 3D hydrogels. Figure 4d–f shows the SEM images of the pore size of 5% GelMA hydrogel, and Figure 4g presents the pore size distribution of 5% GelMA hydrogel. The average pore size of 5% GelMA hydrogel was found to be 14.47 ± 3.73 μm, which lies in the range of GelMA bulk hydrogel pore size at hydrated and lyophilized status (5–200 μm).[41,42]

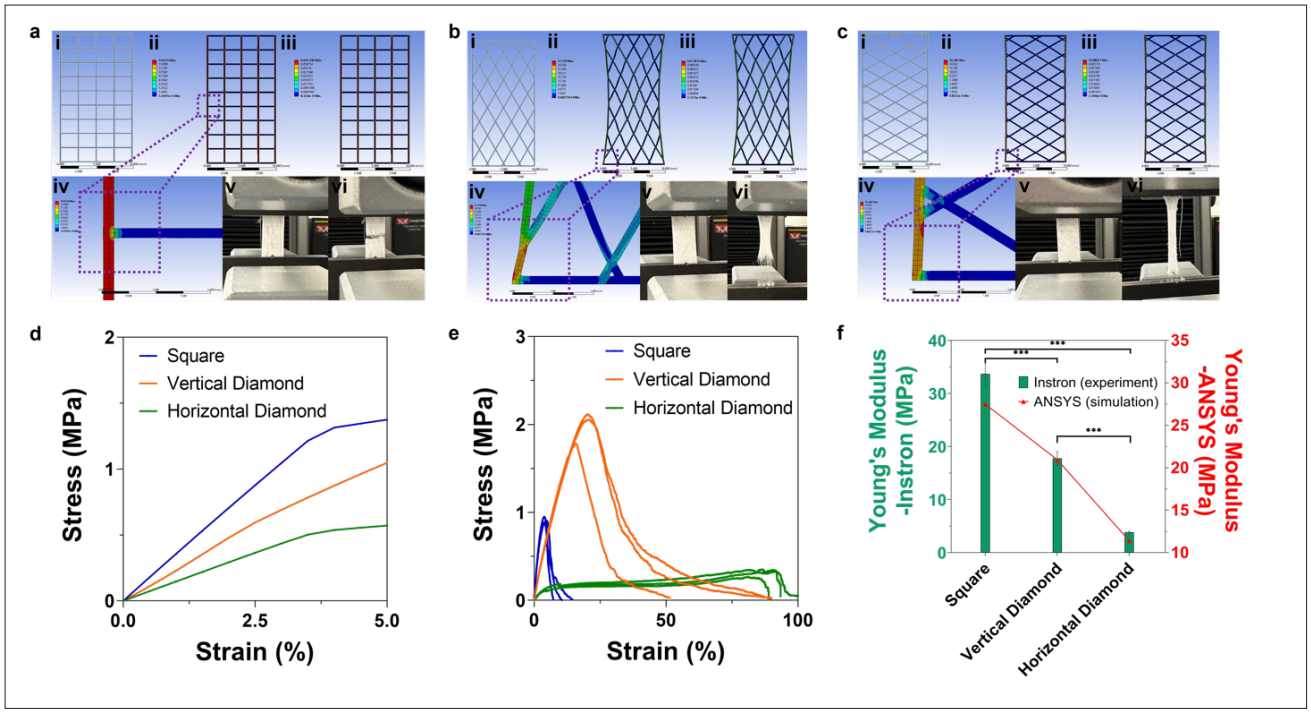

Figure 3. Mechanical properties of three monophasic scaffold patterns. (a–c) The CAD geometry (part i), the equivalent stress (part ii), the equivalent strain (part iii) of the square (a), the horizontal diamond (b), and the vertical diamond patterns (c). (iv) The highest stress area was zoomed in for preview. (v) The initial and (vi) the fracture point of the Instron tensile test. (d) The stress–strain curves generated from ANSYS simulation for each monophasic scaffold pattern. (e) The stress–strain curves generated from physical experiments for each monophasic scaffold pattern. (f) The Young's modulus comparison between the physical experiment group and simulation group of each monophasic scaffold pattern. All data are expressed as mean ± standard deviation. Significance is indicated as ***($p < 0.001$).

Several studies have examined the mechanical properties of the GelMA and its effectiveness on cell behaviors in 3D cell culture models.[43,44] However, whether the mechanical properties of hydrogels attenuate after repeated experiments remain unclear. Figure 4h displays the stress–strain curves of the 5% GelMA hydrogel, encompassing the first compression test up to the 1500th repetition, while Figure 4i summarizes Young's modulus for each repetition.

Remarkably, the Young's modulus of GelMA exhibited only a 5% variation (not significant) from the first to the last compression, emphasizing its excellent stability and repeatability (Figure 4h and i). Furthermore, the Young's modulus of the 5% GelMA falls within the range of 7–7.6 kPa, a range that has been demonstrated to be suitable for mimicking the physiological conditions of brain tissue and providing a compatible environment for NSCs.[45–47]

However, the Young's modulus of GelMA is still much lower than our MEW-printed PCL layer (3.83 MPa), posing challenges in terms of mechanical stability and suturing. To address the limitations of hydrogel-based approaches, Wu et al.[48] introduced a hybrid hydrogel composed of GelMA and silk fibroin glycidyl methacrylate (SF-MA). They found that the additional SF-MA significantly increased the Young's modulus of the hydrogel from 0.027 MPa (GelMA) to 3.51 MPa (SF-MA), approaching the mechanical properties of PCL.

However, PCL degrades at a much slower rate than hydrogels, allowing for prolonged structural integrity during *in vivo* regeneration. Therefore, there is an unmet need for combining synthetic polymers and natural polymers to impart the best of both properties—mechanical robustness and ECM mimicry.

3.3. Biofabricating the tri-layered NGC with MEW and extrusion-based bioprinting

As stated earlier, combining synthetic polymers and natural polymers to impart the best of both properties, i.e., mechanical robustness and ECM-mimicking microenvironment, were an interesting idea. However, most of the works as cited earlier, were ineffective, either for not providing directional cues or conferring weaker mechanical properties.[25] In most cases, it was electrospun mats that were combined with hydrogel fillers.[26] The randomness of the electrospun fibers and their poor repeatability were not desirable. To address the challenge of achieving an ECM-mimicking environment

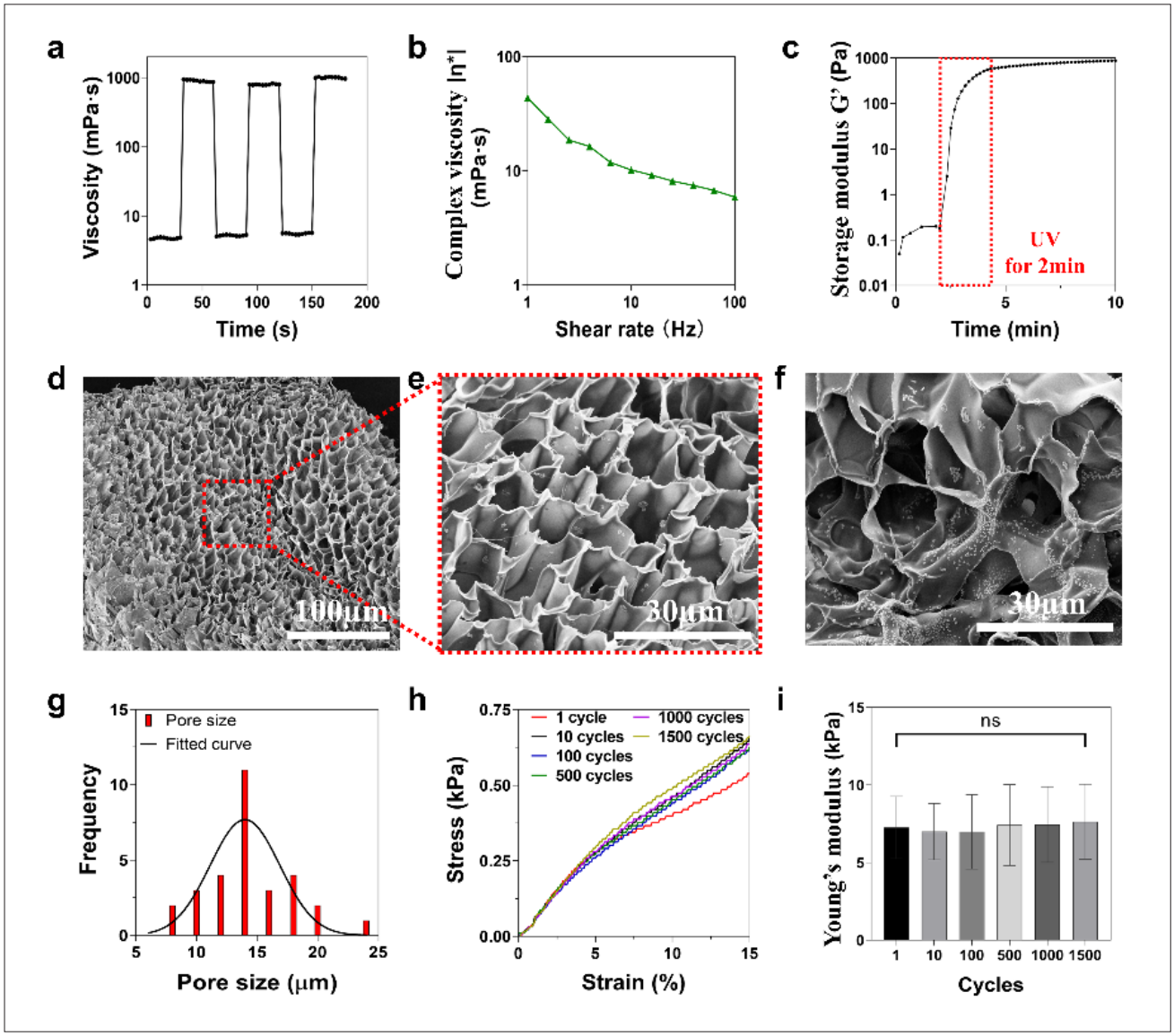

Figure 4. Material characterizations of GelMA before and after crosslinking (a) A three-interval thixotropy test from low shear (0.1 Hz) to high shear rate (100 Hz) cycles of 30 s intervals. (b) The complex viscosity of 5% GelMA solution at a shear rate from 1 to 100 Hz. (c) The storage modulus of 5% GelMA as a function of time (UV on at 2 min and off at 4 min for a duration of 120 s). (d–f) The SEM images displaying both side and top views of the 5% GelMA hydrogel. (g) The pore size distribution of 5% GelMA hydrogel. (h) The stress–strain curves for 5% GelMA hydrogel from the first to the 1500th compression. (i) The Young's modulus of 5% GelMA hydrogel under each repetition ('ns' indicate not significant). All data are expressed as mean ± standard deviation. Abbreviations: GelMA, gelatin methacryloyl; SEM, scanning electron microscopy.

while maintaining robust, predictable, tunable, and repeatable mechanical properties, we introduced a tri-layered NGC fabricated using MEW and extrusion-based bioprinting techniques.

Each NGC can be divided into three different layers and each layer was printed by a distinct 3D printing method (Figure 5a–g). The outer (bottom) layer was printed by MEW with a tool path of mesh structure to enhance the mechanical properties by maximizing the interactions among the fibers. The middle layer was designed to be aligned PCL fibers and printed using MEW, to provide guided cell alignment during axonal regeneration. The inner (top) layer was fabricated by simply extruding a cell-laden GelMA bioink on top of the PCL fibers, followed by UV light crosslinking. The structures were then folded manually into cylinders, sealed with a fibrin glue sealant, and then cultured in the 24-well plate (Figure 5h–l).

It has been reported that neuronal cells tend to be directionally aligned based on the topographical cues to achieve biomimicry.[49,50] For instance, Lee et al.[26] 3D-printed

a micro-grooved surface pattern using gelatin for directional alignment. Limited by the printing resolution of gelatin hydrogel, only seven horizontal struts were printed in the NGC. By leveraging MEW-based 3D printing, we successfully printed densely packed aligned PCL fibers as the middle layer that provides optimal guidance for axonal regeneration (Figure 5b–d).

Furthermore, hydrogels might lose their micro-grooved structure within a few hours to a couple of days, due to their fast degradation or swelling post-implantation *in vivo*, making it ineffective.[51] MEW-printed aligned PCL fibers, on the other hand, offer superior mechanical stability and robustness, ensuring sustained structural integrity to serve as topographical cues crucial for aligned nerve regeneration.

Moreover, the alignment of NGCs is crucial for enhancing neuronal regeneration as it provides topographical cues that facilitate the regeneration of peripheral nerves across long nerve gaps.[50,52,53] Aligned NGCs promote directional axonal growth, reducing random sprouting, and improving the chances of successful target reinnervation.[54,55] Additionally, the migration of Schwann cells, which play a vital role in myelination and nerve repair, is promoted by the aligned fibers, facilitating faster and more organized axonal regrowth.[56,57]

3.4. Tri-layered NGC supports neural stem cell viability and proliferation

Compared to 2D cell cultures, 3D cell culture mimics the *in vivo* conditions representing the natural structure and function of cells within the organism.[58] The encapsulation of cells within 3D hydrogels stands out as the leading method for advancing tissue regeneration efforts.[59] In this study, NSCs were encapsulated in the GelMA hydrogel and subsequently bioprinted as the inner layer (third layer) of the tri-layered structure.

Cell viability within the tri-layered NGC was assessed on days 1, 7, and 14. Figure 6a illustrates the growth of NSCs within the cultured nerve conduits. A substantial increase of cell viability from 76.40% to 90.71% was observed from Day 7 to Day 14, achieving the highest cell viability among all time points (Figure 6b). This observation suggests a favorable environment for cell compatibility and sustained viability within the tri-layered NGCs.

Within 1 day after bioprinting, NSCs were dispersed throughout the hydrogel in various planes and began their attachment to the hydrogel matrix. NSCs represent a type of adherent cell, taking minutes to hours to attach depends on the cell types and surface.[60] During the attachment process, the cells remain viable in suspension. Cells that successfully attach will gradually proliferate, while those that do not attach will eventually die due to the lack of integrin signaling, triggering anoikis.[61,62] By Day 7, NSCs gradually adhered to the hydrogel, adapted to their environment, initiated colony formation, and subsequently started proliferating. In this study, cells were in the attachment process on Day 1, meaning most cells, whether attached or not, remained alive. From Day 2 onward, unattached cells began to die, while attached cells acclimated to the new environment and slowly started to grow. Given that the doubling time for 2D cultured NSCs are 4 days, and it could take even longer time for the 3D culturing NSCs, this led to a relatively low live cell ratio on Day 7.[63] From Day 7 to Day 14, the attached NSCs proliferated and grew, showing the excellent cytocompatibility of the GelMA bioink. By Day 14, the cells continued to grow, resulting in the highest live cell ratio. The results of the proliferation test exhibited a similar trend to the live/dead cell ratio, further corroborating the results.

The AlamarBlue cell proliferation assay provides further evidence of significant cell proliferation from Day 7 to Day 14 (Figure 6c), which aligns with the observed live/dead staining patterns. Specifically, the percentage reduction of AlamarBlue on Day 14 was 1.7-fold ($p < 0.01$) and 2.5-fold ($p < 0.01$) higher compared to Day 1 and Day 7, respectively.

3.5. Tri-layered NGC fosters differentiation of neural stem cells to peripheral neurons

The regulation of differentiation from NSCs to PNs is crucial for developing therapies that enhance neuronal regeneration or synaptic network reconstruction.[64] The essence of nerve regeneration hinges on the ability to transmit neural signals, a process that necessitates robust neuron-to-neuron connections. By effectively guiding the differentiation of NSCs, we can substantially produce more PNs and rebuild the transmission of neural signals, thereby promoting nerve regeneration.

The cultured tri-layered NGC's immunofluorescence staining revealed the presence of the PN marker NEFH, prominent in neuron axons, by Day 14 (Figure 6d). This suggests that the NSCs underwent differentiation into peripheral neurons on the scaffolds with the PN induction media. qPCR was conducted to assess the expression of PN-specific markers *PRPH* and *NEFH*, alongside the stemness marker *HNK1*, on Days 3 and 14 post-differentiation (Figure 6e). On Day 14, post-PN induction, the relative mRNA expression of *PRPH* and *NEFH* increased by 4.4-fold ($p < 0.01$) and 2.79-fold ($p < 0.01$), respectively, compared to the Day 3 samples. This is consistent with the observed decline in the expression of the stemness marker HNK1 from Day 3 to Day 14. The diminished expression of *HNK1*, a stemness marker, signifies the reduction of NSCs

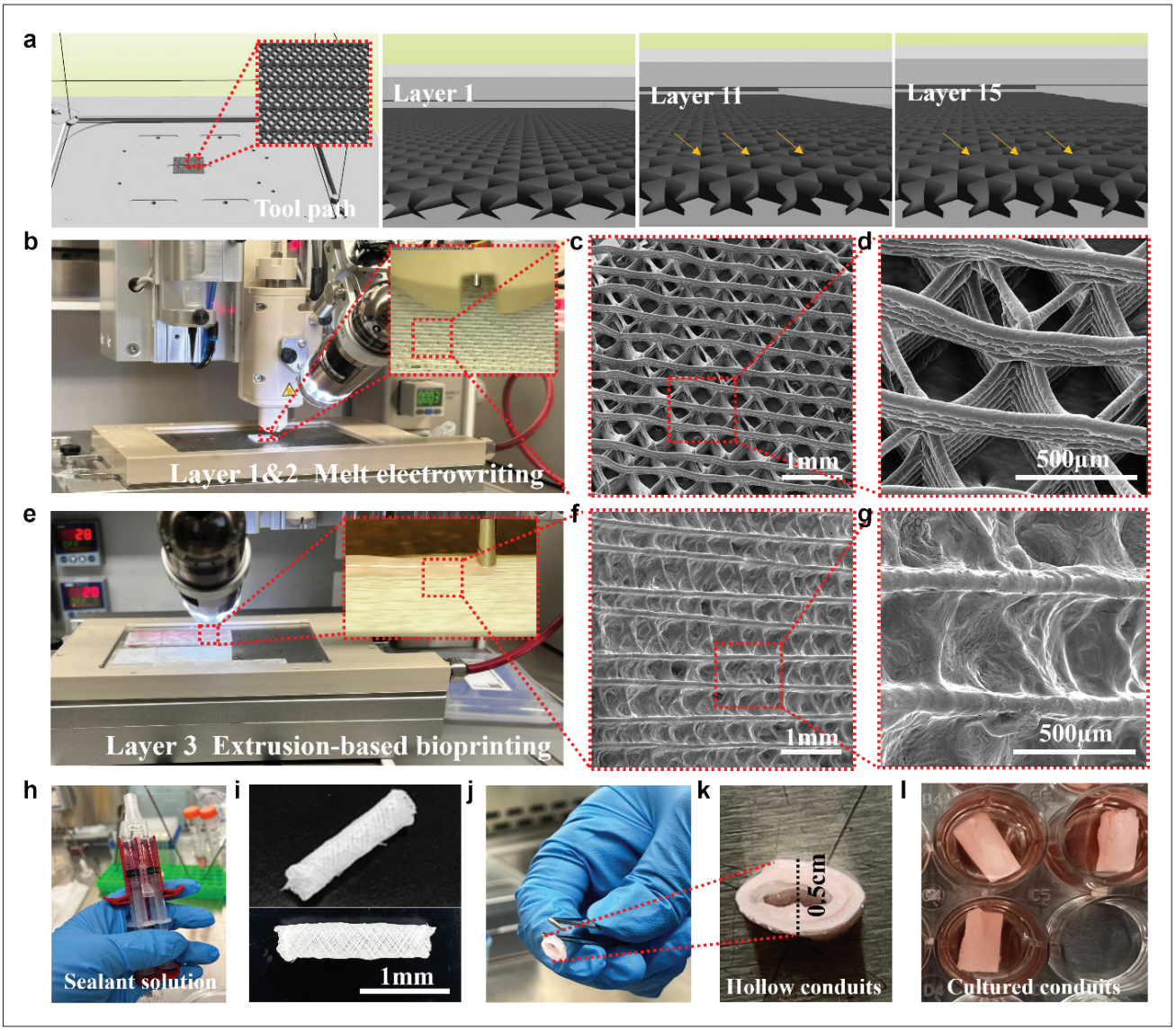

Figure 5. The biofabrication workflow. (a) The CAD design and different layer views of the sample (yellow arrow indicates the aligned fibers). (b) The MEW printing in progress. (c, d) The SEM images of the first and the second MEW-printed layers. (e) The extrusion-based bioprinting in progress. (f, g) The SEM images of the third hydrogel-based layers. (h) The fibrin glue, which performs as a biocompatible adhesive. (i) The dimension of the NGC after rolling and sealing processes. (j, k) The cross-section view of the sealed NGC. (l) The NGCs immersed in the NSC media for cell culture. Abbreviations: CAD, computer-aided design; MEW, melt-electrowriting; NGC, nerve guide conduit; SEM, scanning electron microscopy.

and the differentiation of NSCs into PNs.[9] Additionally, the Day 14 neurons demonstrated a modest increase in *TUBB3* expression levels, with a 25% ($p < 0.05$) increase.

4. Conclusion

In summary, we have successfully designed and biofabricated a tri-layered 3D-bioprinted NGC, with appropriate mechanical robustness, topographical cues for directional alignment, and a cell-encapsulating ECM-mimicking hydrogel environment. The materials chosen (PCL and GelMA) are biocompatible and can be tuned for the controlled delivery of nerve growth factors or other nerve regeneration drugs to further enhance their effectiveness in treating peripheral nerve injuries. With their ease of fabrication, cost-effective materials (PCL and GelMA), and potential for fabricating long conduits, the proposed tri-layered NGCs are very promising candidates for treating long nerve gap injuries.

While our study provides a comprehensive *in vitro* evaluation of the tri-layered NGC, *in vivo* validation

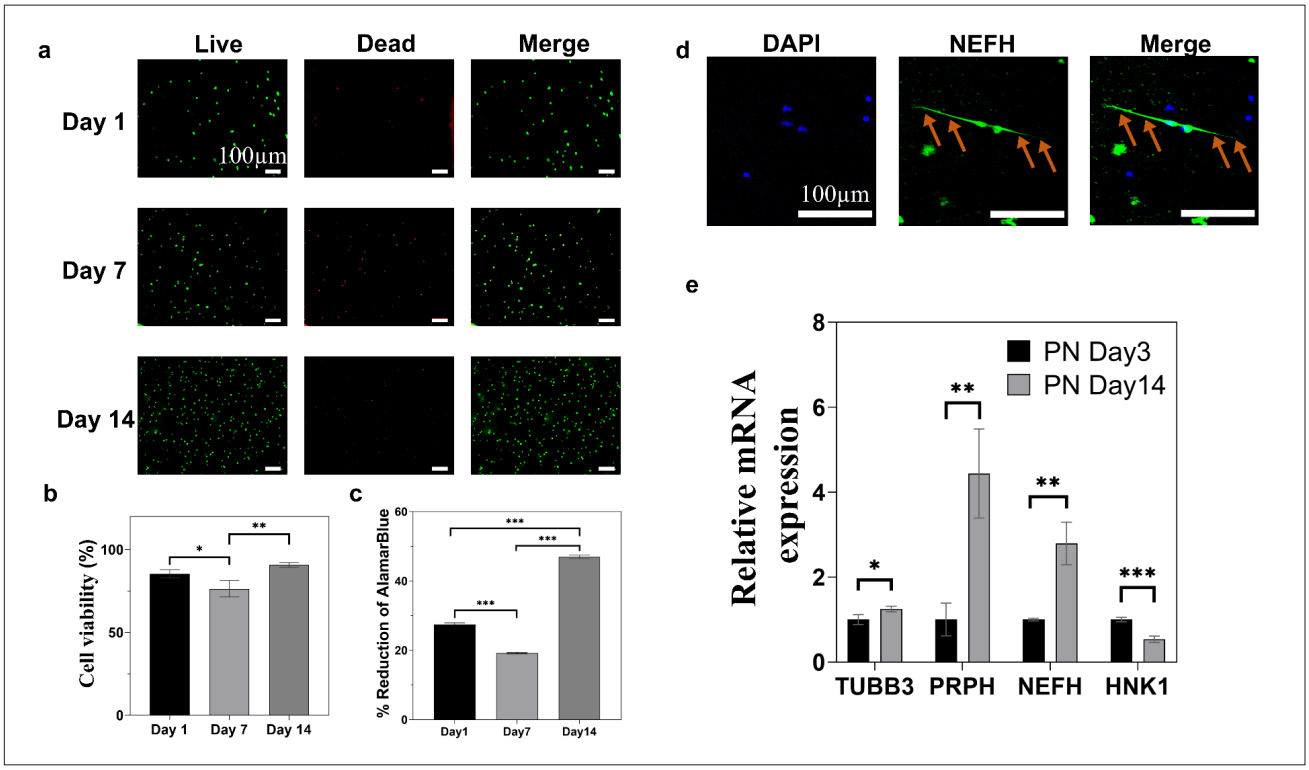

Figure 6. NSCs cultured on tri-layered NGCs (a) The live/dead staining for cell embedded 5% GelMA on Days 1, 7, and 14. (b) The quantification of live and dead cells on Days 1, 7, and 14. (c) The percentage reduction of AlamarBlue reagent from Day 1 to Day 14. (d) The expression of NEFH protein on Day 14 in the induced NSCs-loaded scaffolds (arrows indicate the neurite outgrowth). (e) The gene expression studies using qPCR experiments, including pan-neuronal marker *TUBB3*, PN-specific markers *PRPH* and *NEFH*, and stemness marker *HNK1*. The gene expression was normalized to the expression of housekeeping gene *GAPDH*. All data are expressed as mean ± standard deviation. Significance is indicated as *($p < 0.05$), **($p < 0.01$), and ***($p < 0.001$). Abbreviations: GAPDH, glyceraldehyde 3-phosphate dehydrogenase; HNK1, human natural killer 1; NEFH, neurofilament heavy polypeptide; PN, peripheral neuron; PRPH, peripherin; qPCR, quantitative polymerase chain reaction; TUBB3, Tubulin beta 3 class III.

remains a crucial next step. Future studies will involve animal models to assess the conduit's long-term biocompatibility, degradation, and functional nerve regeneration *in vivo*. These experiments will provide critical insights into the NGC's ability to support axonal regrowth and integrate with native tissues. Furthermore, these experiments will strengthen the clinical relevance of our findings and further validate the translational potential of our proposed design.

Acknowledgments

This research was partially carried out using the Core Technology Platforms resources at New York University Abu Dhabi.

Funding

This work was supported by the Early-Stage Research Award from the NYU Discovery Research Fund for Human Health to S.V.

Conflict of interest

Sanjairaj Vijayavenkataraman is an Editorial Board Member of this journal, but was not in any way involved in the editorial and peer-review process conducted for this paper, directly or indirectly. Separately, other authors declared that they have no known competing financial interests or personal relationships that could have influenced the work reported in this paper.

Author contributions

Conceptualization: Jiarui Zhou, Sanjairaj Vijayavenkataraman
Formal analysis: Jiarui Zhou, Kamil Elkhoury
Fund acquisition: Sanjairaj Vijayavenkataraman
Investigation: Jiarui Zhou
Methodology: Jiarui Zhou, Kamil Elkhoury, Soja Saghar Soman
Project administration: Sanjairaj Vijayavenkataraman
Validation: Jiarui Zhou, Kamil Elkhoury
Visualization: Jiarui Zhou

Writing–original draft: Jiarui Zhou
Writing – review and editing: Kamil Elkhoury, Sanjairaj Vijayavenkataraman
All the authors read and approved the manuscript.

Ethics approval and consent to participate

Not applicable.

Consent for publication

Not applicable.

Availability of data

All data generated or analyzed during this study are included in this published article.

References

1. Kuffler DP, Foy C. Restoration of neurological function following peripheral nerve trauma. *Int J Mol Sci*. 2020;21(5):1808.
doi: 10.3390/ijms21051808

2. Qiao F, Jeongsim H, Shuxin L. Nonsteroidal anti-inflammatory drugs promote axon regeneration via RhoA inhibition. *J Neurosci*. 2007;27(15):4154.
doi: 10.1523/JNEUROSCI.4353-06.2007

3. Maugeri G, D'Agata V, Trovato B, et al. The role of exercise on peripheral nerve regeneration: from animal model to clinical application. *Heliyon*. 2021;7(11):e08281.
doi: 10.1016/j.heliyon.2021.e08281

4. Kornfeld T, Vogt PM, Radtke C. Nerve grafting for peripheral nerve injuries with extended defect sizes. *Wien Med Wochenschr*. 2019;169(9):240-251.
doi: 10.1007/s10354-018-0675-6

5. Soman SS, Vijayavenkataraman S. Perspectives on 3D bioprinting of peripheral nerve conduits. *Int J Mol Sci*. 2020;21(16):5792.
doi: 10.3390/ijms21165792

6. Gao Y, Wang Y-l, Kong D, et al. Nerve autografts and tissue-engineered materials for the repair of peripheral nerve injuries: a 5-year bibliometric analysis. *Neural Regen Res*. 2015;10(6):1003-1008.
doi: 10.4103/1673-5374.158369

7. Ouyang L, Armstrong James PK, Lin Y, et al. Expanding and optimizing 3D bioprinting capabilities using complementary network bioinks. *Sci Adv*. 2020;6(38):eabc5529.
doi: 10.1126/sciadv.abc5529

8. Elkhoury K, Morsink M, Tahri Y, et al. Synthesis and characterization of C2C12-laden gelatin methacryloyl (GelMA) from marine and mammalian sources. *Int J Biol Macromol*. 2021;183:918-926.
doi: 10.1016/j.ijbiomac.2021.05.040

9. Soman S, Govindraj M, Al Hashimi N. Bioprinting of human neural tissues using a sustainable marine tunicate-derived bioink for translational medicine applications *Int J Bioprint*. 2022;8(4):604.
doi: 10.18063/ijb.v8i4.604

10. Govindharaj M, Al Hashemi NS, Soman SS, Vijayavenkataraman S. Bioprinting of bioactive tissue scaffolds from ecologically-destructive fouling tunicates. *J Clean Prod*. 2022;330:129923.
doi: 10.1016/j.jclepro.2021.129923

11. Elkhoury K, Morsink M, Sanchez-Gonzalez L, Kahn C, Tamayol A, Arab-Tehrany E. Biofabrication of natural hydrogels for cardiac, neural, and bone tissue engineering applications. *Bioact Mater*. 2021;6(11):3904-3923.
doi: 10.1016/j.bioactmat.2021.03.040

12. Van Den Bulcke AI, Bogdanov B, De Rooze N, Schacht EH, Cornelissen M, Berghmans H. Structural and rheological properties of methacrylamide modified gelatin hydrogels. *Biomacromolecules*. 2000;1(1):31-38.
doi: 10.1021/bm990017d

13. Chen Z, Wang L, Chen C, et al. NSC-derived extracellular matrix-modified GelMA hydrogel fibrous scaffolds for spinal cord injury repair. *NPG Asia Mater*. 2022;14(1):20.
doi: 10.1038/s41427-022-00368-6

14. Kim J, Raja N, Choi YJ, et al. Enhancement of properties of a cell-laden GelMA hydrogel-based bioink via calcium phosphate phase transition. *Biofabrication*. 2024;16(1):015010.
doi: 10.1088/1758-5090/ad05e2

15. Yue K, Trujillo-de Santiago G, Alvarez MM, Tamayol A, Annabi N, Khademhosseini A. Synthesis, properties, and biomedical applications of gelatin methacryloyl (GelMA) hydrogels. *Biomaterials*. 2015;73:254-271.
doi: 10.1016/j.biomaterials.2015.08.045

16. Xu W, Molino BZ, Cheng F, et al. On low-concentration inks formulated by nanocellulose assisted with gelatin methacrylate (GelMA) for 3D printing toward wound healing application. *ACS Appl Mater Interfaces*. 2019;11(9):8838-8848.
doi: 10.1021/acsami.8b21268

17. Petcu EB, Midha R, McColl E, Popa-Wagner A, Chirila TV, Dalton PD. 3D printing strategies for peripheral nerve regeneration. *Biofabrication*. 2018;10(3):032001.
doi: 10.1088/1758-5090/aaaf50

18. Jin Z, Li Y, Yu K, et al. 3D printing of physical organ models: recent developments and challenges. *Adv Sci*. 2021;8(17):2101394.
doi: 10.1002/advs.202101394

19. O'Neill KL, Dalton PD. A decade of melt electrowriting. *Small Methods*. 2023;7(7):e2201589.
doi: 10.1002/smtd.202201589

20. Kim J, Bakirci E, O'Neill KL, Hrynevich A, Dalton PD. Fiber bridging during melt electrowriting of poly(ε-Caprolactone) and the influence of fiber diameter and wall height. *Macromol Mater Eng*. 2021;306(3):2000685. doi: 10.1002/mame.202000685

21. Weekes A, Wehr G, Pinto N, et al. Highly compliant biomimetic scaffolds for small diameter tissue-engineered vascular grafts (TEVGs) produced via melt electrowriting (MEW). *Biofabrication*. 2023;16(1):015017. doi: 10.1088/1758-5090/ad0ee1

22. Keßler L, Mirzaei Z, Kade JC, Luxenhofer R. Highly porous and drug-loaded amorphous solid dispersion microfiber scaffolds of indomethacin prepared by melt electrowriting. *ACS Appl Polymer Mater*. 2023;5(1):913-922. doi: 10.1021/acsapm.2c01845

23. Akhtar R, Sherratt MJ, Cruickshank JK, Derby B. Characterizing the elastic properties of tissues. *Mater Today*. 2011;14(3):96-105. doi: 10.1016/S1369-7021(11)70059-1

24. Caliari SR, Burdick JA. A practical guide to hydrogels for cell culture. *Nat Methods*. 2016;13(5):405-414. doi: 10.1038/nmeth.3839

25. Takeya H, Itai S, Kimura H, et al. Schwann cell-encapsulated chitosan-collagen hydrogel nerve conduit promotes peripheral nerve regeneration in rodent sciatic nerve defect models. *Sci Rep*. 2023;13(1):11932. doi: 10.1038/s41598-023-39141-2

26. Lee HS, Jeon EY, Nam JJ, et al. Development of a regenerative porous PLCL nerve guidance conduit with swellable hydrogel-based microgrooved surface pattern via 3D printing. *Acta Biomater*. 2022;141:219-232. doi: 10.1016/j.actbio.2022.01.042

27. Fadia NB, Bliley JM, DiBernardo GA, et al. Long-gap peripheral nerve repair through sustained release of a neurotrophic factor in nonhuman primates. *Sci Transl Med*. 2020;12(527):eaav7753. doi: 10.1126/scitranslmed.aav7753

28. Elkhoury K, Sanchez-Gonzalez L, Lavrador P, et al. Gelatin methacryloyl (GelMA) nanocomposite hydrogels embedding bioactive naringin liposomes. *Polymers*. 2020;12(12):2944. doi: 10.3390/polym12122944

29. Chen T, Xia Y, Zhang L, et al. Loading neural stem cells on hydrogel scaffold improves cell retention rate and promotes functional recovery in traumatic brain injury. *Mater Today Bio*. 2023;19:100606. doi: 10.1016/j.mtbio.2023.100606

30. Vijayavenkataraman S, Kannan S, Cao T, Fuh JYH, Sriram G, Lu WF. 3D-printed PCL/PPy conductive scaffolds as three-dimensional porous nerve guide conduits (NGCs) for peripheral nerve injury repair. *Front Bioeng Biotechnol*. 2019;7:266. doi: 10.3389/fbioe.2019.00266

31. Frost HK, Andersson T, Johansson S, et al. Electrospun nerve guide conduits have the potential to bridge peripheral nerve injuries in vivo. *Sci Rep*. 2018;8(1):16716. doi: 10.1038/s41598-018-34699-8

32. Gao S, Tang Y, Sun W, et al. 3D-bioprinted GelMA nerve guidance conduits promoted peripheral nerve regeneration by inducing trans-differentiation of MSCs into SCLCs via PIEZO1/YAP axis. *Mater Today Adv*. 2023;17:100325. doi: 10.1016/j.mtadv.2022.100325

33. Borschel GH, Kia KF, Kuzon WM, Dennis RG. Mechanical properties of acellular peripheral nerve. *J Surg Res*. 2003;114(2):133-139. doi: 10.1016/S0022-4804(03)00255-5

34. Ju M-S, Lin C-CK, Fan J-L, Chen R-J. Transverse elasticity and blood perfusion of sciatic nerves under in situ circular compression. *J Biomech*. 2006;39(1):97-102. doi: 10.1016/j.jbiomech.2004.10.026

35. Xiao S, Zhao T, Wang J, et al. Gelatin methacrylate (GelMA)-based hydrogels for cell transplantation: an effective strategy for tissue engineering. *Stem Cell Rev Rep*. 2019;15(5):664-679. doi: 10.1007/s12015-019-09893-4

36. Shahidi S, Janmaleki M, Riaz S, Sanati Nezhad A, Syed N. A tuned gelatin methacryloyl (GelMA) hydrogel facilitates myelination of dorsal root ganglia neurons in vitro. *Mater Sci Eng C*. 2021;126:112131. doi: 10.1016/j.msec.2021.112131

37. Ye W, Li H, Yu K, et al. 3D printing of gelatin methacrylate-based nerve guidance conduits with multiple channels. *Mater Design*. 2020;192:108757. doi: 10.1016/j.matdes.2020.108757

38. O'Connell CD, Zhang B, Onofrillo C, et al. Tailoring the mechanical properties of gelatin methacryloyl hydrogels through manipulation of the photocrosslinking conditions. *Soft Matter*. 2018;14(11):2142-2151. doi: 10.1039/C7SM02187A

39. Annabi N, Nichol JW, Zhong X, et al. Controlling the porosity and microarchitecture of hydrogels for tissue engineering. *Tissue Eng Part B Rev*. 2010;16(4):371-383. doi: 10.1089/ten.teb.2009.0639

40. Murphy CM, O'Brien FJ. Understanding the effect of mean pore size on cell activity in collagen-glycosaminoglycan scaffolds. *Cell Adhes Migr*. 2010;4(3):377-381. doi: 10.4161/cam.4.3.11747

41. Yin H, Zhu M, Wang Y, Luo L, Ye Q, Lee BH. Physical properties and cellular responses of gelatin methacryloyl bulk hydrogels and highly ordered porous hydrogels. *Front Soft Matter*. 2023;2;1101680. doi: 10.3389/frsfm.2022.1101680

42. Gu L, Li T, Song X, et al. Preparation and characterization of methacrylated gelatin/bacterial cellulose composite hydrogels for cartilage tissue engineering. *Regen Biomater*. 2020;7(2):195-202.

doi: 10.1093/rb/rbz050

43. Yin B, Yang H, Yang M. Integrating soft hydrogel with nanostructures reinforces stem cell adhesion and differentiation. *J Compos Sci*. 2022;6(1):19. doi: 10.3390/jcs6010019

44. Merivaara A, Koivunotko E, Manninen K, et al. Stiffness-controlled hydrogels for 3D cell culture models. *Polymers*. 2022;14(24):5530. doi: 10.3390/polym14245530

45. Fan L, Liu C, Chen X, et al. Directing induced pluripotent stem cell derived neural stem cell fate with a three-dimensional biomimetic hydrogel for spinal cord injury repair. *ACS Appl Mater Interfaces*. 2018;10(21):17742-17755. doi: 10.1021/acsami.8b05293

46. Mijailovic AS, Galarza S, Raayai-Ardakani S, et al. Localized characterization of brain tissue mechanical properties by needle induced cavitation rheology and volume controlled cavity expansion. *J Mech Behav Biomed Mater*. 2021;114:104168. doi: 10.1016/j.jmbbm.2020.104168

47. Weltman A, Yoo J, Meng E. Flexible, penetrating brain probes enabled by advances in polymer microfabrication. *Micromachines (Basel)*. 2016;7(10):180. doi: 10.3390/mi7100180

48. Wu W, Dong Y, Liu H, et al. 3D printed elastic hydrogel conduits with 7,8-dihydroxyflavone release for peripheral nerve repair. *Materials Today Bio*. 2023;20:100652. doi: 10.1016/j.mtbio.2023.100652

49. Li A, Hokugo A, Yalom A, et al. A bioengineered peripheral nerve construct using aligned peptide amphiphile nanofibers. *Biomaterials*. 2014;35(31):8780-8790. doi: 10.1016/j.biomaterials.2014.06.049

50. Kim Y-t, Haftel VK, Kumar S, Bellamkonda RV. The role of aligned polymer fiber-based constructs in the bridging of long peripheral nerve gaps. *Biomaterials*. 2008;29(21):3117-3127. doi: 10.1016/j.biomaterials.2008.03.042

51. Hawkins AM, Milbrandt TA, Puleo DA, Hilt JZ. Synthesis and analysis of degradation, mechanical and toxicity properties of poly(β-amino ester) degradable hydrogels. *Acta Biomater*. 2011;7(5):1956-1964. doi: 10.1016/j.actbio.2011.01.024

52. Sarker M, Naghieh S, McInnes AD, Schreyer DJ, Chen X. Strategic design and fabrication of nerve guidance conduits for peripheral nerve regeneration. *Biotechnol J*. 2018;13(7):e1700635. doi: 10.1002/biot.201700635

53. Carvalho CR, Oliveira JM, Reis RL. Modern trends for peripheral nerve repair and regeneration: beyond the hollow nerve guidance conduit. *Front Bioeng Biotechnol*. 2019;7:337. doi: 10.3389/fbioe.2019.00337

54. Zhang K, Zheng H, Liang S, Gao C. Aligned PLLA nanofibrous scaffolds coated with graphene oxide for promoting neural cell growth. *Acta Biomater*. 2016;37:131-142. doi: 10.1016/j.actbio.2016.04.008

55. Yang S, Zhu J, Lu C, et al. Aligned fibrin/functionalized self-assembling peptide interpenetrating nanofiber hydrogel presenting multi-cues promotes peripheral nerve functional recovery. *Bioact Mater*. 2022;8:529-544. doi: 10.1016/j.bioactmat.2021.05.056

56. Puhl DL, Funnell JL, Nelson DW, Gottipati MK, Gilbert RJ. Electrospun fiber scaffolds for engineering glial cell behavior to promote neural regeneration. *Bioengineering*. 2020;8(1):4. doi: 10.3390/bioengineering8010004

57. Zhao Y, Liang Y, Ding S, Zhang K, Mao H-q, Yang Y. Application of conductive PPy/SF composite scaffold and electrical stimulation for neural tissue engineering. *Biomaterials*. 2020;255:120164. doi: 10.1016/j.biomaterials.2020.120164

58. Knight E, Przyborski S. Advances in 3D cell culture technologies enabling tissue-like structures to be created in vitro. *J Anat*. 2015;227(6):746-756. doi: 10.1111/joa.12257

59. Wenzhuo F, Ming Y, Liyang W, et al. Hydrogels for 3D bioprinting in tissue engineering and regenerative medicine: Current progress and challenges. *IJB*. 2023;9(5):759. doi: 10.18063/ijb.759

60. Naganuma T. The relationship between cell adhesion force activation on nano/micro-topographical surfaces and temporal dependence of cell morphology. *Nanoscale*. 2017;9(35):13171-13186. doi: 10.1039/c7nr04785a

61. Sater AP, Rael LT, Tanner AH, et al. Cell death after traumatic brain injury: detrimental role of anoikis in healing. *Clin Chim Acta*. 2018;482:149-154. doi: 10.1016/j.cca.2018.04.008

62. Taddei ML, Giannoni E, Fiaschi T, Chiarugi P. Anoikis: an emerging hallmark in health and diseases. *J Pathol*. 2011;226(2):380-393. doi: 10.1002/path.3000

63. Kanemura Y, Mori H, Kobayashi S, et al. Evaluation of *in vitro* proliferative activity of human fetal neural stem/progenitor cells using indirect measurements of viable cells based on cellular metabolic activity. *J Neurosci Res*. 2002;69(6):869-879. doi: 10.1002/jnr.10377

64. An J, Chen B, Tian D, Guo Y, Yan Y, Yang H. Regulation of neurogenesis and neuronal differentiation by natural compounds. *Curr Stem Cell Res Ther*. 2022;17(8):756-771. doi: 10.2174/1574888X16666210907141447